

An Ion Trap For Cavity QED

Tan Kok Chuan Bobby

April 4, 2010

*An academic exercise presented in partial fulfilment for the degree
of Bachelor of Science with Honours in Physics*

Supervisor: Asst. Prof. BARRETT, Murray Douglas

Department of Physics

National University of Singapore

2009/2010

Acknowledgements

I would like to give thanks to everyone in the microtraps group who have helped me in one way or another. This thesis would not have been possible without all their help over the past few months.

I would especially like to thank my supervisor, Asst. Prof Murray, for his patient guidance and for giving me this opportunity to experience physics research first hand.

Special thanks as well to the PhD Students Boon Leng and Nick, for stopping me before I break things.

Abstract

In this Thesis, we discuss the design, construction and commissioning on a linear Paul trap used to trap Barium ions. The operating principles of the trap and the laser cooling techniques are explained. We also outline the technical details and methodology used to successfully trap Barium ions. The work done in this thesis provides the foundations needed for future research towards the use of trapped ions for quantum information processing.

Contents

1	Introduction	6
2	The Theoretical Basis For Paul Trap Confinement, Ion Detection, and the Laser Cooling of Trapped Ions	8
2.1	The Quadrupole Field	8
2.2	The Pseudopotential	10
2.3	Ion Detection Through Resonance Florescence from Single Ions	13
2.3.1	Dark States	15
2.4	Laser Cooling of Trapped Ions	19
3	Ion Trap Components and Experimental Setup	26
3.1	Design and Construction of the Linear Ion Trap	26
3.2	The Vacuum System	29
3.3	The Helical Resonator	34
3.4	The Ion Dispensing System	37
3.5	The Laser Cooling and Detection System	40

4	Ion Trapping Methodology, Observations, and Results	43
4.1	Ion Trapping Methodology	43
4.1.1	Operating Parameters and Ion Trapping Procedure	43
4.1.2	Experimental Issues and Troubleshooting	45
4.2	Results and Discussions	47
5	Conclusion, Summary of Experience and Future Directions of The Project	52

Chapter 1

1 Introduction

Within a modern practical computer, information is encoded as a string of bits, with each bit corresponding to either a “0” or “1” state at any point in time. A quantum computer on the other hand, carries the information via “quantum” bits. It is quantum in the sense that rather than simply occupy either a “0” state or a “1” state at any one time, it is possible to induce a quantum system to occupy any superposition (or linear combination) of the “0” and “1” states. This quantum bit of information, each containing a linear combination of states, is also called a “qubit”. Due to the nature of quantum mechanics, a qubit is inherently probabilistic. It is precisely this kind of indeterministic property of a qubit which allows for new kinds of computing possibilities and for new ways for computer algorithms to work. One example of such an algorithm was invented by Shor[1], for finding the period of a periodic function.

A practical realization of a qubit can be in the form of a trapped atom or an ion, which can be made to occupy different quantum states through the manipulation of lasers. This project aims to construct and trap an ion for the eventual manipulation of its qubit state. The primary advantage of trapping ions as opposed to trapping atoms is that for an ion, due to the nature of its electric charge, it is easier to achieve a stronger confinement and a larger trap depth, which in turn benefits the trap stability and lifetime. The specific kind of trap which was constructed is a radio frequency ion trap, or otherwise also called a Paul trap. A Paul Trap employs the use a radio frequency(RF) potential, in combination with a DC potential, to contain an ion close to the center of the

trap. The Paul Trap was first proposed by Wolfgang Paul *et al.* in 1959[14], but was initially treated as a kind of a novelty until the 1980s, where it will form an integral part in fundamental atomic physics experiments, and its applications would eventually grow to include spectroscopy, frequency standards, g-factor and mass measurements, collision studies and lifetime measurements. In 1989, Paul would eventually receive a Nobel Prize for his work on the ion trap, sharing the prize with Dehmelt and Ramsey[6].

The RF drive for a Paul trap is usually within the few hundred volts at the megahertz or tens of megahertz regime. This may be provided by a commercial function generator followed by an amplifier and a resonator to step up the amplitude of the RF. The RF, in tandem with a static potential, produces an effective pseudopotential which traps the ion near to the center of the trap. The ions will then oscillate about within the pseudopotential in what is called the “macromotion” of the ions. Ions a distance away from the center of the trap will experience an additional “micromotion” due to the fluctuating RF potential. The two different kinds of motion, micromotion and macromotion, will be important considerations for how well the ion can be trapped and eventually cooled.

The outline for this thesis will be as follows. In Chapter 2, the basic theoretical framework for a linear Paul trap, the ion detection system, and the laser cooling system will be outlined. Chapter 3 will then provide a description of all the essential components of the Paul trap, which include the trap structure itself, the vacuum system, the RF driver, the ion dispensing system, and the ion detection system. Chapter 4 will then go into the actual trapping methodology, and discussions of observations. Chapter 5 will then conclude this thesis by summarizing the most important results and discuss about the future direction of the project.

Chapter 2

2 The Theoretical Basis For Paul Trap Confinement, Ion Detection, and the Laser Cooling of Trapped Ions

2.1 The Quadrupole Field

The linear Paul Trap confines an ion by using a dynamic time dependent quadrupole field. The primary motivation for using a dynamic potential rather than a static one comes from Earnshaw's Theorem[5], which states that it is not possible to form an electric potential with a stable equilibrium using any configuration of static charges. Consider first a quadrupole field potential ϕ in a given three-dimensional space. In Cartesian coordinates the potential would then be given by

$$\phi = \frac{\phi_0}{2r_0^2}(\lambda x^2 + \sigma y^2 + \gamma z^2) \quad (1)$$

where ϕ_0 is the magnitude of the external applied potential, r_0 is related to the actual physical geometry of the trap, and λ, σ, γ are multiplicative constants dependent on the applied field. Such a potential can be ideally realized by the following electrode configuration:

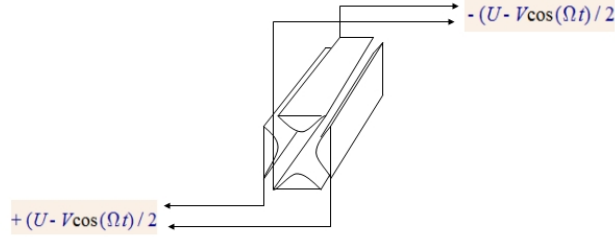


Figure 1: Ideal electrode structure for generating a quadrupole field. The curved surface of the electrodes are hyperbolic, and the potential applied to each electrode is of the opposite polarity with the adjacent electrode. In this configuration, r_0 is simply the closest distance between the trap center to the surface of the electrode, and $\phi_0/2$ is simply the magnitude of the potential on the surface of the electrode

Given that this is an electric potential, it must therefore satisfy Laplace's equation for electrostatics

$$\nabla^2 \phi = \frac{\phi_0}{2r_0^2} (2\lambda + 2\sigma + 2\gamma) = 0 \quad (2)$$

Which, except in the trivial case where $\phi_0 = 0$, suggests that

$$\lambda + \sigma + \gamma = 0 \quad (3)$$

and also implies a well known result - the quadrupole field configuration gives rise to a saddle point potential, which is a point of unstable equilibrium. In order to circumvent this issue and to allow a quadrupole field to be able to confine an ion, the Paul Trap creates a pseudopotential by dynamically varying the quadrupole field with time.

2.2 The Pseudopotential

We now consider adding a RF time dependence to the quadrupole field. When we begin to add a time dependence to the quadrupole potential, supposing that the time dependence oscillates fast enough, the ion would begin to feel the effects of an 'effective potential' called the pseudopotential. The pseudopotential is not the actual electrostatic potential seen by the ion at any point in time, but rather, it is the potential felt by the ion over a longer time scale and governs the large oscillatory motion of the ion when it is within the trapping region of the Paul Trap. The expression for the potential, with an oscillatory time dependence, is the following

$$\Phi(\vec{x}, t) = \phi(\vec{x}) \sin(\Omega t) \quad (4)$$

where Ω is the frequency of the RF applied. Intuitively, we would expect that a trapped ion would have a large macromotion due to oscillations within the pseudopotential and an additional, smaller, micromotion associated with the fast RF jittering in the quadrupole field. We can therefore separate the motion of the ion within this time dependent potential into two parts: a small amplitude oscillation called $\vec{\delta}(t)$ and a larger macromotion called $\vec{Z}(t)$, where $\delta \ll Z$ and $\ddot{Z} \ll \ddot{\delta}$. The equation of motion will then take the form:

$$m(\ddot{\vec{Z}} + \ddot{\vec{\delta}}) = e\mathbf{E}(\vec{Z} + \vec{\delta}) = e\vec{\nabla}\phi(\vec{x}) \sin(\Omega t) \quad (5)$$

As is the usual case for finding points of stable equilibrium, we now apply a multivariate Taylor's expansion (up to the second order) to the quantity ϕ , which is the static potential in the absence of the RF modulation.

$$\phi(\vec{x}) = \phi(\vec{Z} + \vec{\delta}) \approx \phi(\vec{Z}) + (\vec{\nabla}\phi(\vec{Z}))^T(\vec{\delta}) + \frac{1}{2}\vec{\delta}^T H_\phi \vec{\delta} \quad (6)$$

Where H_ϕ is the Hessian matrix of $\phi(\vec{x})$, defined to be:

$$H_\phi = H_\phi(\vec{Z}) = \begin{pmatrix} \partial_{xx}\phi & \partial_{xy}\phi & \partial_{xz}\phi \\ \partial_{yx}\phi & \partial_{yy}\phi & \partial_{yz}\phi \\ \partial_{zx}\phi & \partial_{zy}\phi & \partial_{zz}\phi \end{pmatrix} \quad (7)$$

The equation of motion of the ion can therefore be rewritten using the Taylor's expansion as

$$\begin{aligned} m(\ddot{\vec{Z}} + \ddot{\delta}) &= e\vec{\nabla}\phi(\vec{x})\sin(\Omega t) \\ &\approx e\vec{\nabla}[\phi(\vec{Z}) + (\vec{\nabla}\phi(\vec{Z}))^T(\delta) + \frac{1}{2}\delta^T H_\phi \delta]\sin(\Omega t) \end{aligned} \quad (8)$$

However, since $\delta \ll Z$ and $\ddot{\vec{Z}} \ll \ddot{\delta}$, we can make the following approximations to simplify the expression

$$\begin{aligned} m\ddot{\delta}(t) &\approx e[\vec{\nabla}\phi(\vec{Z})]\sin(\Omega t) \\ &= -\mathbf{E}\sin(\Omega t) \end{aligned} \quad (9)$$

Which allows for a simple solution for the micromotion of the ion. Solving for the micromotion $\vec{\delta}(t)$ we obtain

$$\vec{\delta}(t) = -\frac{e}{m\Omega^2}\mathbf{E}(\vec{Z})\sin(\Omega t) \quad (10)$$

We can now insert this expression into the equation 8 and by taking the time average, it is possible to solve for the macromotion of the particle, which is the motion most directly concerned with the trapping of the ion. We will then

obtain the following differential equation

$$\begin{aligned}\ddot{\vec{Z}} &= -\frac{e^2}{2m\Omega^2}H(\vec{Z})\mathbf{E}(\vec{Z}) = -\frac{e^2}{4m^2\Omega^2}\vec{\nabla}|\vec{\nabla}\phi(x)|^2 \\ &= -\frac{1}{m}\vec{\nabla}U_{pseudo}\end{aligned}\quad (11)$$

Where U_{pseudo} is the pseudopotential seen by the ion and is defined to be

$$U_{pseudo} = \frac{e^2}{4m\Omega^2}|\vec{\nabla}\phi(x)|^2 \quad (12)$$

With the pseudopotential now known, it is now possible to verify that an oscillating quadrupole potential does indeed provide a point of stable equilibrium which allows an ion to be trapped. In view of simplicity, we verify the case for a 2 dimensional quadrupole potential configuration, which would yield the following expressions

$$\begin{aligned}U_{pseudo} &= \frac{e^2}{4m\Omega^2}|\vec{\nabla}\phi(x)|^2 \\ &= \frac{e^2}{4m\Omega^2}|\vec{\nabla}[\frac{\phi_0}{2r_0}(x^2 - y^2)]|^2 \\ &= \frac{e^2}{2m\Omega^2}\frac{\phi_0^2}{r_0^2}(x^2 + y^2)\end{aligned}\quad (13)$$

This is simply the equation for a 2 dimensional potential well with curvature $\frac{e^2}{2m\Omega^2}\frac{\phi_0}{r_0}$. So the quadrupole potential does indeed give us a stable equilibrium within the pseudopotential, thus allowing us to confine an ion close to the trap center.

2.3 Ion Detection Through Resonance Florescence from Single Ions

Once single have been trapped using the pseudopotential, it becomes necessary to set up some sort of ion detection system. Such an ion detection system is important for the natural reason that an ion is simply too small for the naked eye to see without any external intervention. In particular, one way for an experimenter to detect a trapped ion is to resonantly excite them using a laser of the appropriate frequency. The excited ion would subsequently de-excite from the more energetic state to a less energetic state and emit a photon, causing the ion to fluoresce. If the ions themselves have transition levels that correspond to wavelengths within the visible spectrum, we will be able to detect ions visually by using a simple light sensitive camera focused on the center of the trap. In fact, for the situation where many ions are trapped at the same time, it may even be possible to view an ion cloud with the naked eye. For this reason, Barium ions are used for the experiment, since their resonant lines are in the visible spectrum.

There are two transitions for Barium which are relevant to our ion detection system. The first involves the transition from the ground state of Barium, $6^2S_{\frac{1}{2}}$, to the excited state $6^2P_{\frac{1}{2}}$, and the second transition involves the transition from a lower metastable state, $5^2D_{\frac{3}{2}}$, to the excited state $6^2P_{\frac{1}{2}}$. A simplified energy diagram is included in Figure 2 to illustrate the case.

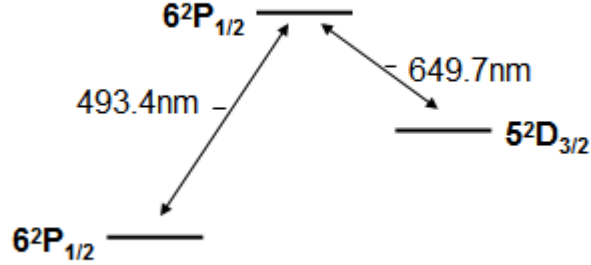


Figure 2: Simplified energy level diagram for a Ba II ion. The $6^2S_{\frac{1}{2}} \longleftrightarrow 6^2P_{\frac{1}{2}}$ transition is the primary excitation for the Barium ion, but there is a chance that the ion may decay into the metastable $5^2D_{\frac{3}{2}}$ state.

The first transition, $6^2S_{\frac{1}{2}} \longleftrightarrow 6^2P_{\frac{1}{2}}$, is the energy level transition which forms the most critical aspect of our ion detection system - this is the primary excitation which will cause the resonant fluorescence of the ion. However, when the ion is excited from the ground $6^2S_{\frac{1}{2}}$ state to the higher $6^2P_{\frac{1}{2}}$ state, there is a chance that it may decay into the metastable $5^2D_{\frac{3}{2}}$ state which has an 80s lifetime. Once an ion is driven into the metastable $5^2D_{\frac{3}{2}}$ state, the resonant fluorescence of the ion essentially stops until the ion once again decays to the ground state and the $6^2S_{\frac{1}{2}} \longleftrightarrow 6^2P_{\frac{1}{2}}$ transition can begin anew, thus preventing the continual observation of the trapped ion.

Measurements of the branching ratio by Davidson *et al.*[13] reveal that there is a 24.4% probability of decay from the excited $6^2P_{\frac{1}{2}}$ into the metastable $5^2D_{\frac{3}{2}}$ state. This suggests that the mean number of $6^2S_{\frac{1}{2}} \longleftrightarrow 6^2P_{\frac{1}{2}}$ transitions that will occur before a random ion will eventually decay into the metastable $5^2D_{\frac{3}{2}}$ state is 3. The implication of this is that each trapped ion will, on average, fluoresce for only a $\sim 0.15\mu\text{s}$ interval before it goes completely dark for 80 sec-

onds, making any meaningful detection of trapped ions difficult or impossible. In order to eliminate this problem of the optical pumping of ions into a dark state, we employ the use of two separate lasers - one laser outputting at 493nm to drive the primary resonant transition $6^2S_{\frac{1}{2}} \longleftrightarrow 6^2P_{\frac{1}{2}}$ for florescence, and another laser at 650nm to act as a repump beam so that any ions can be driven out of the metastable dark states. However, other complications arise from the degenerate energy states of the barium ion, and the 650nm repump beam alone is insufficient to completely eliminate the dark state problem.

2.3.1 Dark States

Much in the same way that the existence of a metastable state makes the trapped ion invisible to the 493nm laser driving the primary resonant transition, there exist states which are dark with respect to the 650nm repump laser. When the ion is driven to such a dark state by decaying from an excited state, the repump process would essentially stop, causing the 650nm laser to be unable to drive the ion back into the ground state for florescence. This is clearly an undesirable situation for ion detection. These dark states are the degenerate Zeeman sublevels of the metastable $5^2D_{\frac{3}{2}}$ state, and the reason why they are 'dark' are primarily due to the selection rules for atomic dipole transitions.

Consider the case where there is a given transition between two energy levels, and we are trying to excite the atom from a lower energy state to a higher energy state using a laser with a certain fixed laser polarization. If the lower energy state has a greater number of Zeeman sublevels than the higher energy state, dark states will naturally occur as some of the Zeeman sublevels of the lower energy state will have no pathways available for it to excite into. In particular for this experiment, a 650nm laser repump ions by exciting the $5^2D_{\frac{3}{2}} \longleftrightarrow$

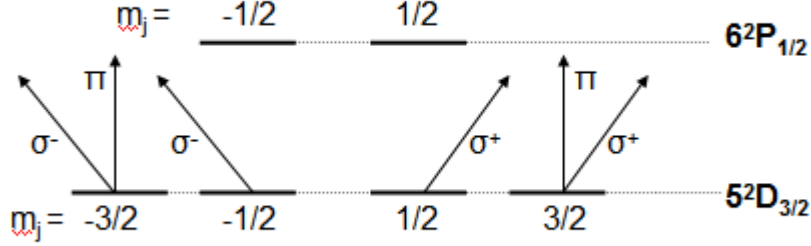


Figure 3: Diagram indicating the dark states for σ^- , π and σ^+ polarized light within the $5^2D_{\frac{3}{2}} \longleftrightarrow 6^2P_{\frac{1}{2}}$ transition. The arrows without a Zeeman sublevel connected at the end indicate that the state is 'dark' for that particular polarization.

$6^2P_{\frac{1}{2}}$ transition. This implies that our lower energetic state, the metastable $5^2D_{\frac{3}{2}}$ state, has 4 Zeeman sublevels corresponding to the angular momentum quantum numbers $m_j = -\frac{3}{2}, -\frac{1}{2}, \frac{1}{2}$ and $\frac{3}{2}$. The more energetic $6^2P_{\frac{1}{2}}$ state have 2 Zeeman sublevels corresponding to the angular momentum quantum numbers $m_j = -\frac{1}{2}$ and $\frac{1}{2}$. Since the lower energy state has more Zeeman sublevels than the higher energetic state, there will be dark Zeeman states which once the ion occupies, will render the ion invisible to the 650nm repump beam of a particular polarization. Figure 3 illustrates the various dark states for different laser polarizations within the $5^2D_{\frac{3}{2}} \longleftrightarrow 6^2P_{\frac{1}{2}}$ transition.

From Figure 3, it can be seen that for either σ^- , π or σ^+ polarized light, there exists 2 Zeeman sublevels in the $5^2D_{\frac{3}{2}}$ metastable state which are dark towards that particular polarization. As an example, for π polarized light, the dark states are $|J = \frac{3}{2}, m_J = \pm\frac{3}{2}\rangle$ as there are no corresponding $|J = \frac{1}{2}, m_J = \pm\frac{3}{2}\rangle$ sublevels in the $6^2P_{\frac{1}{2}}$ state for it to excite into. In the more general case, it is not necessarily true that there will always be 2 dark states for each polarization. Table 1 provides a more complete description of the conditions for the existence

Upper Level	Lower Level	
J_f	Integer J_i	Half-integer J_i
$J_i + 1$	No dark state	No dark state
J_i	One dark state for any polarization	One dark state for each circular polarization
$J_i - 1$	Two dark states for any polarization	Two dark states for any polarization

Table 1: Table listing the conditions for the existence of dark states for arbitrary atomic systems and laser polarizations

of dark states for arbitrary atomic systems and laser polarization in the absence of a magnetic field[3].

There are two methods for the elimination of these dark states. The first of these involves the modulation of the polarization of the 650nm repump beam. The motivation for doing this is because the specific Zeeman sublevels which are dark is dependent on the polarization of the incident radiation, as can be seen in Figure 3. Since the dark states corresponding to the σ^+ polarization are not the same Zeeman sublevels as the dark states for the σ^- polarization, it is possible to simply flip between the two different polarizations continuously so that the ion is never invisible to the incident radiation for an prolonged period of time. For example, if an ion is driven to the $|J = \frac{3}{2}, m_J = +\frac{3}{2}\rangle$ dark state while the incident radiation has a σ^+ polarization, switching the polarization to σ^- would allow the repump beam to interact with the ion once again since the $|J = \frac{3}{2}, m_J = +\frac{3}{2}\rangle$ Zeeman sublevel is not a dark state for σ^- polarized radiation. One concern when modulating the polarization of the incident radiation is that the frequency must be fast enough if the repump is to be efficient - modulating the frequency too slowly results in the ion remaining in the dark state for a longer interval before the 'flipping' of the polarization occurs. A modulation frequency of a few megahertz is generally acceptable.

An alternative method to eliminate the dark state is through the application of a constant magnetic field to the ion. Consider the case where an applied magnetic

field defines a particular quantization axis for the ion. If the laser makes a small angle with the quantization axis, that is, the laser is not exactly aligned with the magnetic field, then the dark states are some linear superposition of the Zeeman sublevels defined by the quantization axis of the magnetic field. In applying a magnetic field to the ion, the degeneracy in the Zeeman sublevels is lifted as each sublevel's energy is shifted non uniformly and the instantaneous dark state would then evolve with time as

$$|\phi(t)\rangle = \sum_{m_i} c_{m_i} |J = \frac{3}{2}, m_i\rangle e^{-i\epsilon_{m_i}t/\hbar} \quad (14)$$

Since each component of the superposition acquires phase at a different rate, the ion will eventually evolve away from the dark state after some time has elapsed, thus allowing the repump beam to interact with the ion once again. This effect can be viewed semiclassically: an ion in a dark state can be viewed as a particular orientation of the ion with respect to the laser. When the ion is in this particular orientation, radiation of a particular polarization cannot interact with the ion due to the selection rules of quantum mechanics, making the ion invisible to the incoming radiation. By applying an additional magnetic field across the ion, it causes the ion to precess about the axis defined by the magnetic field, changing the orientation of the ion and thus moving the ion out of the dark state to interact with the incident radiation once again. Generally, the a magnetic field of a few gauss is sufficient to eliminate the dark states.

For this particular experiment, both polarization modulation and an external magnetic field is employed in the elimination of the dark states as either methods are simple to prepare and set up. With the dark state problem solved in this way, and direct visual observation of the ions now possible, it is then possible to employ laser cooling techniques to cool the trapped ions

2.4 Laser Cooling of Trapped Ions

There are several reasons why the cooling of trapped ions is desirable, the first of which concerns the ionic fluorescence. Hot ions generally have high kinetic energies which result in very large amplitudes of oscillations within the trap. As each ion can only provide a limited amount of fluorescence, a larger amplitude of oscillation would imply that the ion would appear dimmer, as a limited amount of fluorescence is now spread out over a much larger area. Another problem with very large amplitudes of oscillations is that the beam radius of the lasers are only of a limited size, typically around $\sim 100\mu m$. If the amplitude of oscillation is much larger than this, then the ion could spend a significant period of time outside of the radius of the laser or even avoid the laser beam altogether, depending on the kinds of orbits that the ions are traversing. This would significantly compromise our ability to continually observe a trapped ion.

The second reason why cold ions are generally more favored is because hot ions have high moving velocities, which enhances both first order and second order Doppler effects. While the Doppler effect is not in itself necessarily undesirable - it is in fact instrumental to the laser cooling system - it does have a major effect on all spectroscopy related experiments. For instance, it is possible to control which isotope of barium you wish to be trapped by tuning the laser frequencies to heat up certain isotopes and not others. The various isotope shifts of the energy levels ensure that laser frequencies that are resonant for one isotope are far detuned for some other isotope of barium[9]. Due to the variations in the velocities of hot ions, such control over the different isotopes of barium would not be possible as isotopes which previously had large detunings from the laser can now compensate for the detuning through the Doppler effect. The only way to solve this problem is to cool the ions to a sufficiently low temperature such

that the contribution due to the Doppler effect is diminished.

The act of cooling refers to the active decrease of the velocity or kinetic energy of the ions, as the temperature of an ion is a quantity that is closely related to its overall velocity. Whilst there are a wide variety of known methods that are available to cool trapped ions, for the purpose of this project, we employ the Doppler method of laser cooling the ion because it is the easiest to implement - setting up the laser cooling system requires nothing more than the lasers which are already set up for the detection system. Using this method of laser cooling of ions, it is possible to achieve temperatures of the order of mK.

The essential idea of Doppler laser cooling is simple. We first consider the simple case of a two level ion. It is a well known fact that light is composed of numerous photons and each photon possesses a tiny pocket of momentum given by the expression $\hbar \vec{k}$, where \vec{k} is the wave vector of the photon in the direction of the laser beam. Supposing that the laser is on resonance and incident on the ion, the ion would interact with the photons and get excited to a higher energy state. Each of this photon which is absorbed by the ion provides a tiny 'kick' to the ion along the direction of the laser beam as the momentum of the photon is transferred over to the ion during the absorption process. The two level ion will eventually re-emit a photon of exactly the same wavelength, but because the spontaneous emission of photons is isotropic, the direction of the spontaneously emitted photon is completely random and their net effect is zero. If we average out the effect over many absorption-emission cycles, the net force, also called the radiation force, is along the direction of the laser beam and is described by the expression

$$\vec{F} = \hbar \vec{k} \sigma \Gamma \tag{15}$$

Where Γ is the natural line width of the transition, and σ is the average popu-

lation of the excited state. From atomic physics, the average population of the excited state is known to be[7]

$$\sigma = \frac{s/2}{1 + s + (2\delta/\Gamma)^2} \quad (16)$$

Where δ is the detuning of the laser from the resonant frequency, and s is the saturation parameter defined by

$$s = \frac{I}{I_s} \quad (17)$$

$$I_s = \frac{\pi h c \Gamma}{3 \lambda^3} \quad (18)$$

and I_s is called the saturation intensity.

However, Equation 16 is the expression for an ion at rest. Supposing that the ion is instead moving about with a velocity \vec{v} , then with respect to the frame of reference of the moving ion, the ion would perceive a Doppler shift in the incident radiation. Considering only first order Doppler effects, this is equivalent to the substitution of the detuning term, δ , for the following expression

$$\delta = \delta_0 - \vec{k} \cdot \vec{v} \quad (19)$$

Where δ_0 is the laser detuning with respect to an ion at rest. If we set the laser parameters such that $\delta_0 < 0$, that is, by setting the laser such that it is slightly red detuned with respect to the resonant transition at rest, the detuning term δ is only equal to zero when the ion is moving in the opposite direction to the

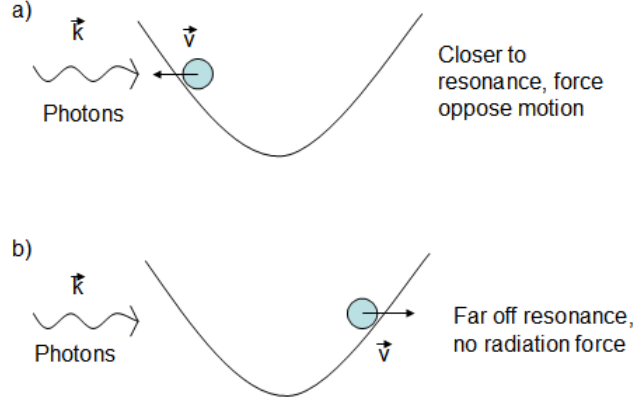


Figure 4: Diagram illustrating the Doppler effect on radiation force for an oscillating ion. In (a), the ion is moving opposite to the direction of the photon, and experiences a radiation force opposite to its motion. In (b), the ion is moving in the same direction as the photons, and do not experience a radiation force as it is off resonance.

directional vector \vec{k} of the laser. Conversely, the detuning term gets increasing large in magnitude when the ions velocity is along the same direction as \vec{k} . The interpretation is that when the ion is moving towards the laser source, it perceives itself to be getting closer towards resonance and it experiences a radiation force opposite to its motion. When the ion is moving away from the laser source, it perceives itself to be getting further and further away from resonance, and the radiation force subsides. What this amounts to is a kind of damping effect on the motion of an oscillating ion - the ion only experiences an overall net force acting against its motion, but never experiences a net force acting in the same direction as its motion. It is in this manner that the ion can be slowed down and cooled. The situation is briefly summarized in Figure 4.

It is worth noting at this point though that the process does not continue indefinitely, and at some minimum temperature, this cooling process will eventually

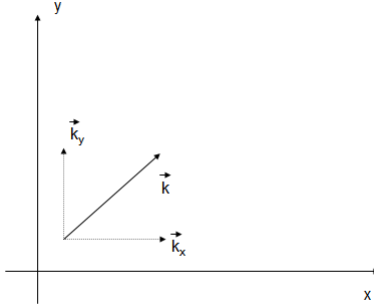


Figure 5: A vector \vec{k} pointing in an oblique angle to the axes can be broken down into its vector components \vec{k}_y and \vec{k}_x , which are parallel to the y and x axes respectively. So the single vector \vec{k} is equivalent to having two vectors \vec{k}_y and \vec{k}_x , each parallel to a different axis.

reach its limit. The fundamental cooling limit for techniques similar to this is called the Doppler limit, and it is given by

$$T_D = \frac{\hbar\Gamma}{2k_B} \quad (20)$$

Where T_D is the lowest possible temperature that can be achieved, Γ is the natural line width of the transition, and k_B is the Boltzmann constant. For the $6^2S_{\frac{1}{2}} \longleftrightarrow 6^2P_{\frac{1}{2}}$ transition in barium which we are using for the experiment, this corresponds to a Doppler cooling limit of $\sim 0.4\text{mK}$.

While the the laser cooling method appears at this point to cool the ion only along one particular direction, it is in fact not necessary to use of three lasers to cool a single ion oscillating in the 3 dimensions of the physical space. By simply aligning one laser such that the direction of the beam is oblique to all the principal axes of the trap, it is possible to cool the ion in all 3 directions of its oscillation[8].

This is because by aligning the laser such that it is oblique to all of the principal axes of oscillation of the ion, the k -vector of the laser can be broken down into their vector components, each of which are individually parallel to a separate axes. At least locally, this is mathematically equivalent to using 3 separate lasers with each laser point along a different axial direction, except of course only one laser is being used. The situation is illustrated for a 2-dimensional case in Figure 5, but the same principle equally holds for 3-dimensional space, thus allowing for the cooling of a trapped ion in 3 dimensions using only a single laser.

However, in order for the cooling to be efficient in such a case, there must be no degeneracy of the trap frequencies along all the axes of the trap. This is because when any two or more of the axes have the same trap frequency, the trajectory of the ion will always cross the cooling laser perpendicular to the direction of the laser. This implies that there is no component of the velocity parallel to the direction of the laser whenever the ion reaches the cooling beam, so no cooling can occur due to the absence of the Doppler effect. This is illustrated in Figure 6 for a 2 dimensional case. This problem is easily rectified though, by introducing slight asymmetries to the trap. For example, this can be done by applying a small bias voltage on the DC trap electrodes.

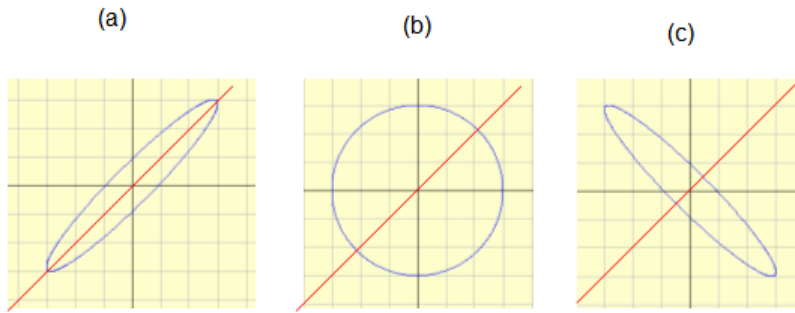


Figure 6: Diagram illustrating the various kinds of trajectory the ion follows when the trap frequencies are degenerate. Diagram (a) illustrates the case where the vertical oscillation lags the horizontal oscillation in phase. Diagram (b) illustrates the case where the vertical oscillation and the horizontal oscillation is in phase. Diagram (c) illustrates the case where the vertical oscillation is ahead of the horizontal oscillation in phase. In all cases, the trajectories are perpendicular to the laser when the ion meets the cooling beam. The laser is represented by the straight line.

Chapter 3

3 Ion Trap Components and Experimental Setup

In this section, the various subsystems of the ion trap are described in greater detail. The ion trap itself is composed of many interdependent subsystems, each of which fulfill a specific role which is critical towards the complete functioning of the trap. The various systems include: the vacuum system housing the Paul trap, the RF driver supplying the radio frequency source to the electrodes, the ion dispensing system, and the ion cooling/detection system. The basic construction and design of the linear Paul trap will first be outlined, followed by a description of the vacuum system, the helical resonator, the schemes employed for creating ionized barium, and the laser systems responsible for the ion cooling and detection.

3.1 Design and Construction of the Linear Ion Trap

The linear Paul trap constructed for this ion trapping experiment is of a classical design consisting of 4 metallic rods with a circular diameter as well as 2 end caps being held up by various support structures. In Section 2.1, it is previously mentioned that an ideal electrode configuration for a quadrupole potential are 4 rods whose surfaces are hyperbolic while the Paul trap we've constructed have rods which have a circular radius instead. While it is true that Hyperbolically shaped electrodes would be ideal, they are not used for the reason that they are difficult to fabricate with precision. Circular rods are able to provide a sufficiently close approximation to the ideal electric potential configuration so

as to achieve a similar effect, so the fact that hyperbolically shaped rods are not used do not really arise as a serious problem. The rods and the end caps are made of stainless steel, which is chosen because of its easy availability, anti-corrosive properties as well as its strength. The 4 rods are arranged such that they are parallel and form the edges of a 3 dimensional rectangular cuboid. Each of the rods are separated from their nearest neighbors by 3.6mm and are 1.25mm in diameter. The end caps, on the other hand are 2mm diameter pins with one rounded edge. These are placed near either ends of the electrodes along the axial direction of the trap, with their rounded edges facing each other 7.1mm apart. As an additional feature, a thin aluminum base plate that is 4mm by 4mm made is also placed below the trap center, so that we can adjust the height of ion by applying an additional potential in the vertical direction.

The rods and end caps are supported by posts made of aluminum. Aluminum is chosen because of its good machining properties and also because it is non-porous and bakeable to relatively high temperatures, making it an ideal structural material for the trap. As the rods and the posts are both electrically conductive, alumina is also used as a spacer to insulate the rods from electrical contact with the post. Alumina is similarly resistant to high temperature, making its vacuum property excellent, and it is a relatively hard and stiff material, good for supporting the rods in a fixed position. A tiny amount of epoxy is used to hold the rods and alumina in place and prevent them from sliding out of position, while the end caps, not requiring electrical insulation from the post, is held in place simply by friction alone through precise machining of the parts. Electrical connections to the rods are achieved by crimping a length of copper wire to the ends of the electrodes, while connections to the end cap is achieved by electrifying the entire post through a screw at the bottom of the post. The post is itself supported by a base made of macor, once again chosen because of

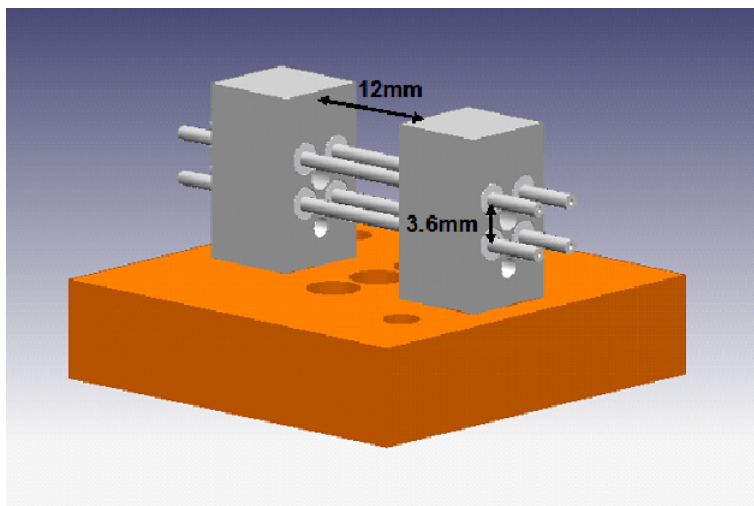


Figure 7: A 3D drawing of the trap design. 4 rods insulated by alumina are slotted into holes machined into 2 rectangular blocks acting as posts supporting the electrode structure. The hole in between the electrodes are intended for the end caps to slide in, and are machined just right such that they can hold the end caps in place purely by friction.

its good machining and vacuum properties. Figure 7 shows 3D drawing of the trap structure illustrating the overall design, while Figure 8 is a picture of the actual trap after it was constructed.

During the construction of the trap, it is imperative that all trap components are fastidiously kept clean, because the trap is intended to operate in an ultra high vacuum environment. Once contaminants on the surfaces of the trap are introduced inside the vacuum system, they can potentially outgas for an indefinite period of time, compromising the quality of our vacuum environment. Contaminants may also cause uncontrolled chemical reactions and provide an avenue for ion loss which cannot easily be detected and rectified once the trap is sealed within the vacuum environment. Another precaution to maintain the quality of the vacuum is that screw holes in the trap are designed with outlets which allow for trapped gases to escape. This is to prevent trapped pockets of

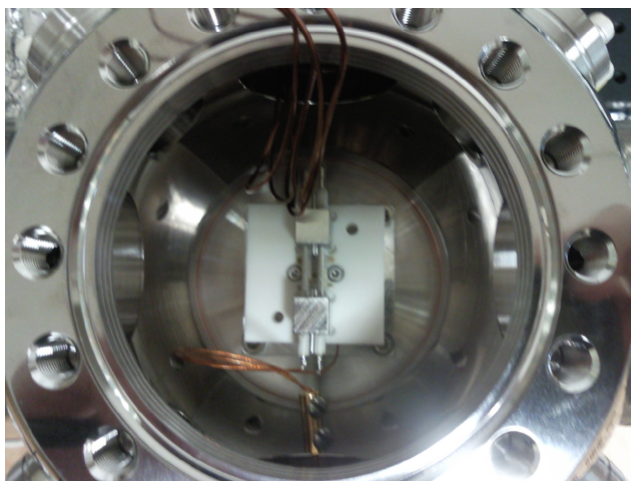


Figure 8: A picture of the actual trap after construction, with electrical connections at the ends of the electrodes.

air once the trap components are screwed in. In an ultra high vacuum environment, such tiny pockets of air may make a significant difference to the quality of the vacuum.

3.2 The Vacuum System

The earliest ion trapping experiments employ a vacuum environment of the order of approximately 10^{-6} Torr to house ion traps. It is ideal that the trap is housed within an environment which is as evacuated of air as possible. This is so as to remove or reduce any avenue for ion losses from the trap. If the ion trap is operating within a less than ideal vacuum environment, the ions will be constantly bombarded by a variety of gas particles. Such collisions are highly undesirable as they will impart energy and momentum to the trapped barium ions, heating them up and of course this will compromise any efforts to cool the ions down. Introducing unknown gases and chemicals within the system may also incidentally result in the trapping of unwanted ions in the trap, or cause

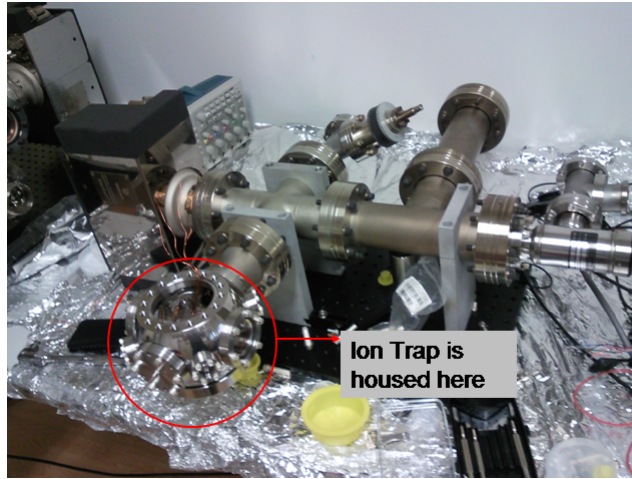


Figure 9: A picture of the vacuum housing. The chamber which will actually contain the ion trap is circled.

unwanted and unpredictable chemical reactions with ionized barium, which can lead to ion losses. As such, present generation ion trapping experiments routinely involve ultra-high vacuums of the order of 10^{-11} Torr. In certain very special cases, even higher vacuum requirements of the order of 10^{-16} or less are involved[11]. For our purpose though, a stabilized pressure of 10^{-10} or 10^{-11} Torr is sufficient.

The vacuum is created within the confines of a vacuum housing, which consists of little more than a series of air-tight pipes and flanges, with connectors and electrical feedthroughs at its ends, where various pumps, power supplies and pressure sensors can be connected. The housing has a chamber with see-through holes and openings which is sealed up using standard quartz-glass windows. This chamber will be where the ion trap is eventually placed when the vacuum housing is evacuated of air. A picture of the vacuum housing before it is pumped down is shown in Figure 9.

Achieving the ultra high vacuum within the housing would require several layers

of processes. The initial pumping down of the vacuum housing is done via a large mechanical pump. This large mechanical pump essentially operates by creating a pressure gradient and imparting momentum to the air particles, directing the air away from the vacuum system and thus evacuating the chamber. In order to aid the evacuation of the chamber, a bakeout period is included in the process. This is because the inner walls of the vacuum system naturally adsorb trace amounts of vapors and gases on its surface, and without intervention, these adsorbed chemicals will continually leak into the surrounding environment at room temperature, potentially for an indefinite period of time. By raising the temperature of the vacuum system to between 150°C to 200°C during the bakeout process, it will accelerate this outgassing process and allow the mechanical pump to pump away these contaminants. This bakeout and mechanical pumping process takes place over the course of approximately 2 days, bringing the pressure down to approximately 10^{-8} Torr. Following this, the pressure is then further reduced by attaching two additional fine pumping systems - the titanium sublimation pump and the ion pump.

Unlike the mechanical pump which injects mechanical momentum into the gas particles in order to direct them away from the vacuum system, the titanium sublimation pump uses a chemical process to further evacuate the system. The remaining gases within the vacuum system which the mechanical pump is unable to pump out of the system is allowed to diffuse on its own towards the titanium sublimation pump. As its name suggests, the sublimation pump contains a sample of titanium which is heated up by a surrounding tungsten filament coil. The coil is heated to the sublimation temperature of titanium, such that a stream of titanium vapor is continuously being given off. These titanium vapors will condense on the cool surrounding chamber, forming a thin layer of deposit on the inner walls. As titanium has a high chemical affinity with hydrogen,



Figure 10: Picture of the bakeout process. The vacuum system is contained within this large metal cage as temperatures are raised to between 150°C to 200°C . The mechanical pump is running continuously as the air inside the chamber is being evacuated. The process takes place over the course of approximately 2 days.

nitrogen, oxygen and all other active gases, any such gas molecules which with the coated portion of the chamber will be bound to the titanium deposits, thus effectively trapping the gas molecule and preventing them from re-entering the vacuum system. The titanium sublimation pump is used primarily to evacuate the vacuum system of hydrogen gas, which is not effectively removed by the mechanical pump.

As a secondary system to further reduce the pressure of the vacuum, an ion pump is also used. Similar to the titanium sublimation pump, the ion pump works not by ejecting gas particles from the vacuum system, but by immobilizing them. Unlike the sublimation pump however, its primary design is not dependent on a chemical process. When a gas molecule enters the ion pump, they get ionized and are quickly accelerated by the large potential gradient, resulting in a high velocity collision with the cathode which embeds the gas

particle below the cathode surface. This effectively traps the gas particles and removes them from the system. As a by-product of the very high velocity of the accelerated ion, when the ion gets embedded in the cathode, sputtering from the electrode surface also occurs. For this reason the cathode for ion pumps are usually composed of titanium. The sputtered titanium will then get deposited on the pump surfaces where they can react with active gases and further aid the removal of gas particles from the system.

Once the vacuum system is pumped down by the titanium sublimation pump and the ion pump, the internal chamber pressure reaches a pressure of about 5×10^{-11} Torr, which is sufficiently low for our experimental requirements. The vacuum system has electrical feedthroughs which allow for electrical connections from outside the chamber and into the trap itself. For the trapping process, 2 of the electrodes and the 2 end caps will be held at constant potential of no more than a few volts. This is readily achieved using standard DC power supplies. The RF supply however, requires more attention, since we would require RF amplitudes of at least several hundred volts in order to achieve sufficiently strong confinement of trapped ions. A typical function generator is only able to generate a sinusoidal signal of several volts in amplitude. Even with the inclusion of a 5 Watt amplifier, the maximum amplitude achievable is only of the order of several tens of volts. Therefore, in order to achieve an even larger voltage amplification, a third stage - a helical resonator - is added to the RF generation to be used in conjunction with the function generator and the amplifier.

3.3 The Helical Resonator

The helical resonator is composed of a single layer inner conductor coiled in the form of a helix enclosed in a hollow conductive shield with a circular cross section. In this experiment, the inner coil is composed of copper, and the outer shield is composed of aluminum, although other conductive materials may also be used. One end of the helical inner conductor is connected directly to the shield, and the other end is connected to the RF electrode feed through. The resonator is fed an RF signal using a simple copper wire looped around the inner conductor and the length of the helix is design to be approximately $1/4$ the wavelength of the desired frequency, which is about 16MHz in this case. When the RF is turned on at the resonant frequency, a standing wave is setup which stores a portion of the energy of the RF and amplifies the input voltage. The voltage near the electrode can be measured by placing a small loop of copper wire at the far end of the helix near the electrode feedthroughs. There is a direct, linear relationship between the EMF generated in the wire loop and the amplitude of the RF, so by calibrating the wire loop to known voltages, it is possible to measure the voltage output of the resonator. Figure 12 is a picture of outer shield of the resonator, while Figure 12 shows a schematic diagram of the resonator showing the inner helix.

The working principle of the resonator is simple - when an RF signal fluctuating at the appropriate resonant frequency is fed into the resonator, a standing wave is set up through the copper helix, which stores a portion of the energy of the input RF, amplifying the voltage amplitude of the incoming signal. Since the helix is designed to be $1/4$ the wavelength of the RF, the end of the helix corresponds to where the amplitude of the standing wave is maximum (see Figure 13); this point can then be tapped to supply the RF to the trap electrodes.

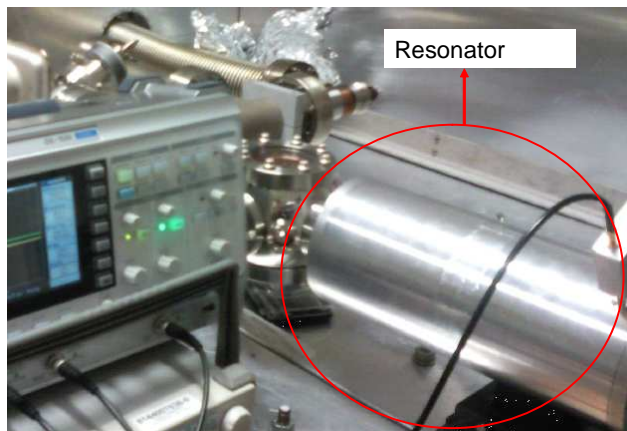


Figure 11: External view of the resonator. It is simply a hollow aluminum tube with a helical coil made of copper inside.

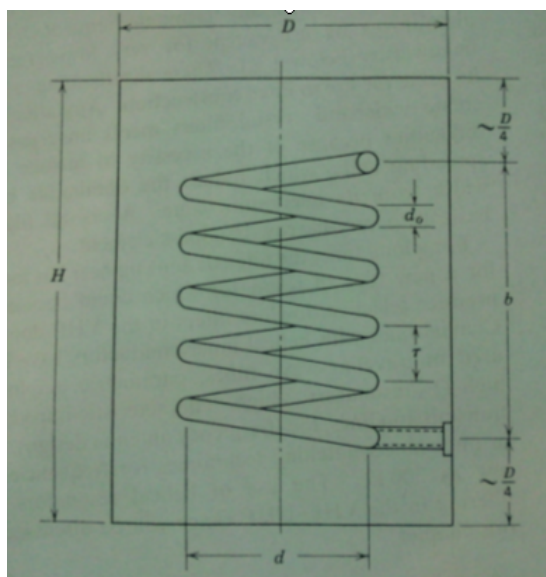


Figure 12: A schematic diagram of the resonator[15]. One end of the helix is connected to the aluminum shield, and the open end is eventually tapped to the RF electrode feedthrough.

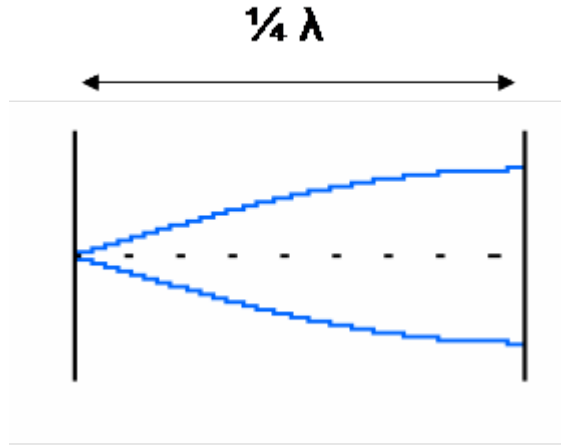


Figure 13: The helix of the resonator is designed to be $1/4$ the length of the RF, generating a standing wave of quarter wavelength at resonance. The maximum amplitude occurs at the end of the helix, which can feed the trap electrodes

In order to maximize the transfer of power from the RF into the resonator, and hence maximize the voltage amplification, we adjust and fine tune the position where the wire loop supplying the RF is connected to the helical coil in order to match the impedance of the load (the impedance of the trap and resonator) with the impedance of the amplifier (50Ω). At the point of impedance matching, the reflection of the signal back to the amplifier is minimized, which is observable on an oscilloscope using a directional coupler. It is appropriate to view the circuit as setting up a damped harmonic oscillator with a forced oscillation driven by the RF input as the helical coil and the electrodes essentially form an L-C circuit. For such forced oscillations of harmonic oscillators, the system can be characterized by a dimensionless quantity called the Q-factor.

The Q factor is a quantity describing how under damped an oscillating system is. Typically, the higher the Q factor, the longer the oscillation will continue after the applied force is turned off. A high Q factor also indicates a lower rate of energy dissipation relative to the energy stored in the resonator, which in turn

leads to a larger voltage amplification at the resonator output. As such, the Q factor is often a useful indicator to compare the quality differences between resonators, as well as an indicator to suggest whether changes and modifications to the resonator has significantly changed its characteristics. A more detailed description of the Q factor is provided in Appendix A.

The measured value of the Q factor of the resonator used in this ion trapping experiment is approximately 140. At this Q factor, the maximum voltage output generated by the resonator is approximately $(900 \pm 100)V$ which is sufficiently large to generate a strong trapping potential along the radial direction on the trap.

3.4 The Ion Dispensing System

An ion trapping experiment naturally requires a source of ions. Ion loading is a two step process - neutral barium atoms is first supplied by a barium oven, following which the neutral atoms can then be ionized and trapped. One of the most common ways to ionize barium, which is also the method adopted for this project, is electron impact ionization. Basically, a beam of electrons is directed towards the center of trap, and the barium atoms would be ionized when an electron collides into it with sufficient force. This beam of electrons is supplied by an electron gun consisting of a length of thoriated tungsten wire. Thoriated tungsten has a reduced work function of 2.6eV, which allows for thermionic emissions of electrons at a lower temperature as compared to ordinary tungsten. The electron surface density of the wire is increased by crimping the wire at a point such that it is bent with a sharp edge. This also allows us to easily choose the direction of the electron beam, as the vast majority of the electron emission will be from the crimped location on the wire. In order the increase the efficiency

of the ionization, a negative bias of 60V[12] is applied to the tungsten wire so that the electrons are accelerated away from the wire at an increased velocity. It is possible to measure how much electrons are being emitted by collecting the electrons on the trap electrodes and measuring the resulting current. A typical current passing through an electron gun is 2.1A, and at this current input, the measured electron beam output is of the order of 100nA.

The neutral barium atoms are supplied by a barium oven. The design of the oven is simple - it is essentially a stainless steel tube with a sample of barium inside. The oven is typically heated to a temperature of approximately 300 to 350 degrees Celsius by passing a current through it, causing barium vapors to rush out of one end of the oven where an opening is cut. Several design variations of the oven were tested, with varying sizes of the openings and locations where the opening was cut, but the optimal design is eventually found to be a single tube with one end left open. This design is illustrated in the 3D drawing shown in Figure 14. A housing made of aluminum was also designed to house the oven and the electron gun, which has holes facing the trap for electrons and barium atoms to be released. This is pictured in Figure 15.

While the initial ion loading phase is achieved by using an electron gun, ion loadings can also be done by shining a broad spectrum Xenon flash lamp into the chamber. By shining light of sufficiently high frequency in the UV range onto the electrode surfaces, the resulting photoelectric emission will be sufficient to ionize the neutral barium within the trap[2]. The flash lamp also contains frequencies which allow it to directly photoionize neutral barium. The benefit of using a flash lamp as opposed to using the electron gun is that it introduces less heat into the chamber and this helps to maintain the low chamber pressure. It is also more difficult to fine tune the amount of thermionic emission that is given off by the electron gun, as the condition of the thoriated tungsten wire can

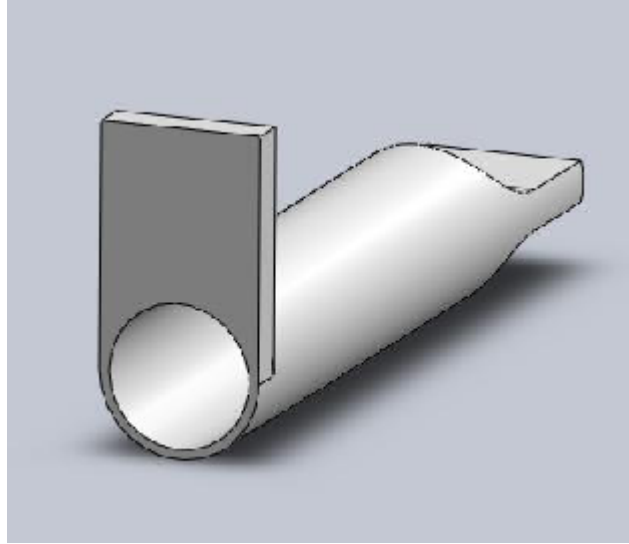


Figure 14: A 3D drawing of the final design of the Barium oven.

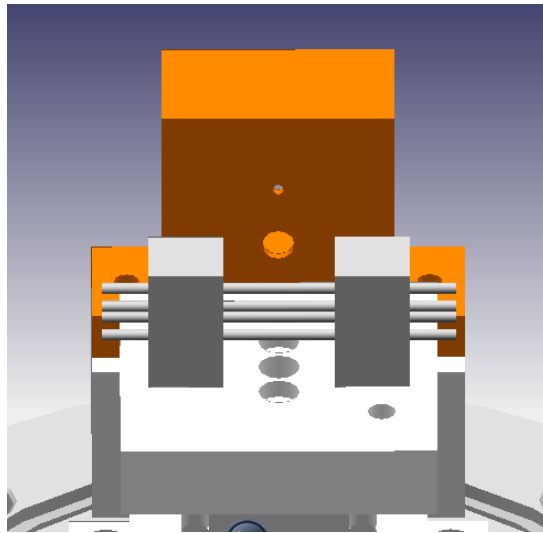


Figure 15: A 3D drawing of the trap together with the housing (highlighted) shielding the Barium oven and electron gun. The smaller hole nearer the top of the housing is for the electron beam to pass through, the larger hole at the bottom is for the Barium vapors.

deteriorate over time. The main benefit of the electron gun is that it is capable of supplying a large electron flux which allows for higher ion loading rates. As such, if a very high loading rate is required, usage of the electron gun may be preferable, but otherwise, if the loading of single ions is desired, the usage of the flash lamp for ion generation is usually preferred.

3.5 The Laser Cooling and Detection System

As was previously described in Sections 2.3 and 2.4, two separate lasers are employed for this ion trapping experiment. These lasers fulfill a dual role of cooling the ions down as well as cause the resonant fluorescence of the ion, and operate at the frequencies 650nm (red) and 493nm (bluish green) respectively. In order to find the correct wavelengths near 493nm and 650nm for the observation of ionic fluorescence, some frequency reference is required so that the lasers can be frequency stabilized at the right frequency. The 650nm laser is locked to an iodine reference line, while the 493 laser is generated by a 986nm source which is locked to a sideband of a cesium reference line and then frequency doubled. Measurements of the frequency is then done using a wave meter which is accurate up to an uncertainty of ± 60 MHz. With the lasers locked, they are then combined into a single beam using a beam splitter and coupled into the same fiber optic cable. Due to the fact that two different frequencies of light are coupled into the same fiber and into the same lens, the focal length and beam waist of the two lasers are different and cannot be individually tuned. The measured beam waist and focal length of the 493nm laser is $28\mu m$ and 105mm respectively, whilst the measured beam waist and focal length of the 650nm laser is $41.5\mu m$ and 140mm respectively. Since the two lasers do not focus at the same point, a compromise was made between the 2 by choosing roughly the midpoint of the two focal lengths to be at the centre of the trap. At

this point, the beam radius for both lasers is $\sim 120\mu m$. With the 493nm laser operating at close to 1mW, and the 650nm operating at close to 500mW, both lasers have sufficient intensity for both the cooling and florescence of the ions at this point. The lasers are initially centered onto the trapping region by moving the laser beam around on a translation stage and taking reference points using the trap electrodes. By taking the average of these reference points, the beam can then be centered correctly. In addition, two acousto-optic modulators are also programmed to switch between two polarizations of the 650nm laser at a frequency of 5MHz. This will serve to eliminate the dark states.

To complete the detection system, a light sensitive CCD camera with a variable focusing lens is set up directly above the chamber housing the trap, enabling us to observe the ionic florescence on a laptop computer screen placed nearby. The CCD camera is fitted with a light filter which filters out wavelengths outside of 493nm, so as to reduce the effect of background radiation on the detection system. The CCD camera is centered into position similar to how the lasers were positioned by using the two end caps as reference points and using the average position as the position over the trap center. Copper wire loops are also placed around the trap, which will act as Helmholtz coil that generates the magnetic field when a current is passed through it. This will serve as a secondary method to eliminate the dark state problem. Figure 16 shows a picture with both the camera mounted on top the the vacuum chamber and the Helmholtz coils surrounding the chamber.

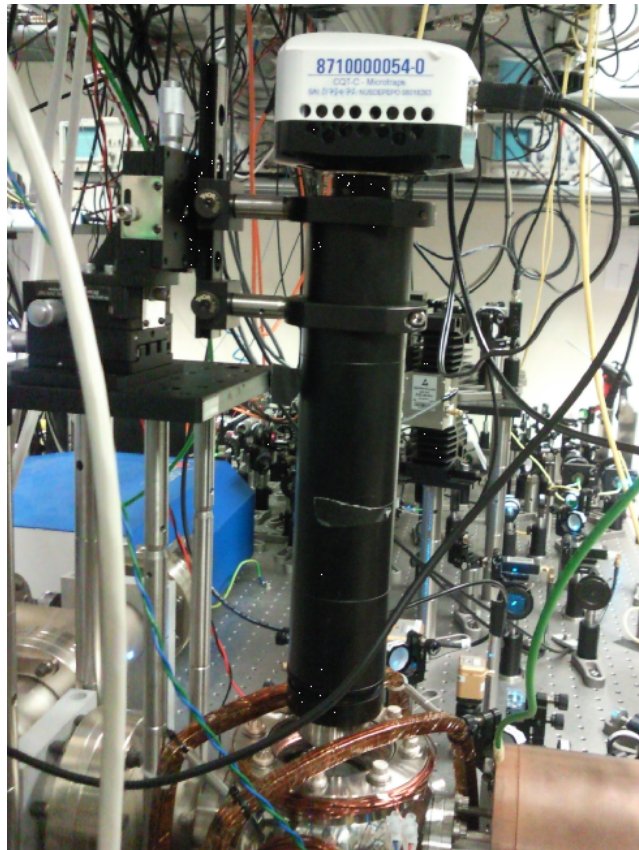


Figure 16: A picture of the CCD camera mounted directly on top of the chamber where the ion trap is housed. The copper wires surround the chamber act as Helmholtz coils to produce a magnetic field that will eliminate the dark states.

Chapter 4

4 Ion Trapping Methodology, Observations, and Results

4.1 Ion Trapping Methodology

4.1.1 Operating Parameters and Ion Trapping Procedure

With all the necessary ion trap components set up and running, the actual ion trapping process is ready to begin. The initial trapping procedure is as follows: First, the DC power supplies and the RF signal generator are switched on to generate the necessary pseudopotential which will provide confinement of the barium ions. The RF supplied to the RF electrodes is operating at the resonance frequency of the resonator, at 15.7MHz, and has an amplitude of approximately 900V. The two end caps and the DC electrodes are held at a constant voltage of -1V and 5 volts respectively, using a standard DC power supply. At these electrode parameters, the trap depth is approximately 19 000K, which is strong enough to provide confinement even for very hot ions.

The primary and the repump lasers are then locked to a point approximately 200MHz red detuned from the expected resonant wavelengths of 493.40768nm and 649.68983nm[10] for the initial loading phase. These are the resonant wavelengths for the isotope Barium 138, which is also the most common isotope of barium. A small red detuning of the frequency is necessary in this case because a blue detuned laser may otherwise heat up the ions and kick them out of the trap, so care must be taken not to be too close to resonance. A 5A current is

then passed through the Helmholtz coil in order to create an approximately 4 Gauss magnetic field at the center of the trap, which should aid the elimination of the dark states, making the florescence of the ions possible.

When an ion is ready to be loaded into the trap, the electron gun and the barium oven are switched on simultaneously, operating at typical currents of 2.3A and 5A respectively. This should generate the ions to be supplied to the trap. As a precaution during the loading phase, the barium oven is made sure not to run continuously over prolonged periods of time, as in doing so we run the risk of prematurely depleting the available barium source. A continuous supply of barium vapor streaming out of the oven can also potentially coat the entire surface of a trap and cause a short circuit between the electrodes. Therefore, for each typical loading of barium ions, the oven is only run for one minute intervals before it is switched off. At this point, if an ion is not yet seen, we allow the chamber pressure to stabilize first before proceeding to tune the various laser parameters and systematically comb through various possible combinations of parameters until ion florescence is observed. Typical parameters adjusted include the individual intensities and the detunings of the 493nm primary laser and the 650nm repump laser, the position of the laser beam, the current passing through the Helmholtz coils, as well as the bias voltage applied to the electron gun. Once the various combinations of parameters are exhausted, the attempt to load barium ions is repeated until ionic florescence is eventually observed.

The goal in the initial loading phases is to be able to trap and observe a large cloud of ions. Once a large cloud is visible, the trap is functioning properly, and the various trap parameters need only to be further fine tuned to stabilize the ions. The fine tuning process begins by first turning down the operating current of the barium oven gradually, such that subsequent loadings on ions yield an increasingly small cloud. The beam position and alignment can be

continually refined by moving the laser position about using the translational stage and maximizing the amount of observed fluorescence from the cloud. As the ion cloud gets increasingly small, the laser is then gradually shifted until it eventually crosses the direct center of the trapping region. With the laser position accurately placed, repeated loadings of barium ions should then be reliably reproducible. At this point, the focus is then placed on fine tuning the rest of the parameters such as the laser detuning, laser intensities, the strength of the magnetic field, and the potential applied to the individual electrodes in order to maximize the amount of fluorescence and to minimize the motion of the ions. Such fine tuning of parameters is done repeatedly over many separate loadings of barium ions, until eventually the trap conditions are such that a small number of stable ions can be trapped stably and in a reproducible manner. Single ions are then loaded into the trap, which can then be subject to further experimentation from this point on.

4.1.2 Experimental Issues and Troubleshooting

There were a variety of issues which were encountered during the various first attempts to trap an ion. Since the Paul trap itself is housed within a vacuum chamber, it is not possible to directly interact with it without first dismantling the vacuum setup. As a result of this, whenever the ion trapping process fails, there were difficulties in isolating the specific problem areas which require attention. While problems with the external setup can easily be identified and quickly remedied, it is not so simple to test the functionality of components housed inside the vacuum chamber. These components include: the end caps and electrodes, the electron gun, and the barium oven. Several indirect methods therefore has to be devised to test these components.

One commonly encountered problem were issues of uncertainty over the electrical connections into the trap electrodes. Since it is not possible to directly probe the inside of the chamber with a multimeter to test whether the electrical connections are working properly, an indirect way to test them is by turning on the electron gun and applying a positive bias to the electrodes or end caps. By applying a positive bias to a particular electrode or end cap, the electron beam should be directed towards that particular electrode/end cap, resulting in a small but measurable current indicating that the electrical connections are closed. In a similar manner, we can also test that the electron gun is functioning properly by ensuring that we measure a current on the electrodes whenever the electron gun is switched on. This is an indication that the electrodes are capturing electrons emitted from the electron gun.

Testing whether the barium oven is working properly is a more complicated process. The typical method employed to check that the oven is working properly is to turn the operating current of the oven up until a brownish black coating is observed on the trap structure surrounding the oven. Once this black coating is observed, it is a sure sign that barium is being given off, and the operating current can be turned down again. However, the use of such a method not entirely desirable as it may cause a thick barium coating to be deposited on the trap surface, potentially causing a short circuit within the trap. There are also issues of subjectivity with this method as it is often unclear whether an observed coating of barium on the trap surface is due to previous unsuccessful loadings of barium ions, or due to the increase in the operating current. As a result of this, the testing of the barium oven is usually performed only when all other possibilities have been exhausted.

If the barium oven is found to be defective, then the vacuum system is dismantled, and the barium oven is replaced, often with certain redesigned aspects

such as modifying the location and size of the opening or changing the geometry of the oven. It is a general observation that the opening where barium vapor comes out of the oven is frequently blocked by barium oxide, which has the appearance of a greyish white powder. This blockage may prevent any further outflow of barium and immediately cuts off the supply of barium into the trap. In consideration of this, the final design of the barium oven (see Figure 14) includes an enlarged opening at one end to reduce the possibility of blockage. It is also necessary to ensure that the barium oven is not exposed to an oxygenated environment for a prolonged period of time to prevent the barium from being oxidised.

4.2 Results and Discussions

The first ion clouds observed within the trap were very diffused and faint. However, this is only to be expected as at the initial loading phase, the trap parameters at this point has yet to be optimized to maximize the amount of florescence. Regardless, this faint cloud is sufficient to serve as a good initial starting point for further refinement. The first observed ion cloud is pictured in Figure 17, and is only just barely perceptible against the black background. Further optimization of the parameters eventually lead to more efficient cooling of the ion clouds and higher levels of florescence. A brighter ion cloud obtained after several more trials is pictured in Figure 18, demonstrating the level of improvement after repeated attempts. The ion cloud in Figure 18 can actually be observed to condense in real time from the large dim cloud into the bright spot seen on the picture, providing a clear indication that the Doppler cooling system is functioning properly. It is also an interesting observation that an ion cloud of this size (estimated to be $\sim 400\mu\text{m}$ across in the radial direction) can be directly observed with the naked eye by simply looking into the trap.



Figure 17: The first ion cloud observed in the Paul trap. The cloud is barely perceptible, and appears as a large diffused cloud at the center of the picture.

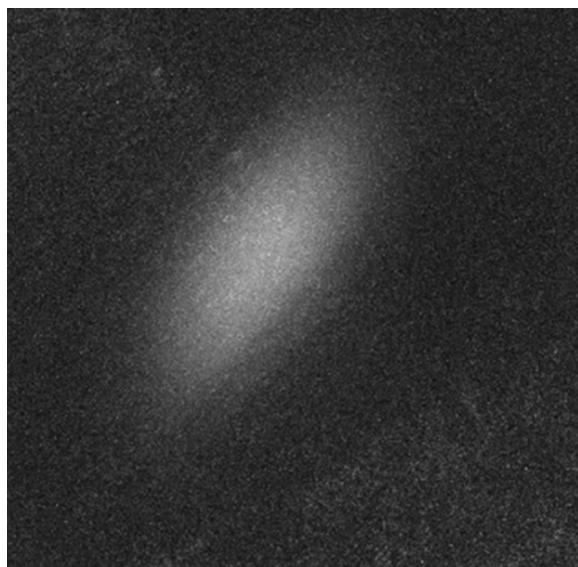


Figure 18: A brighter cloud is observed after several fine tunings of the parameters. The cloud in this picture is larger than the size of the laser beam, leading to what appears to be an asymmetric shape.

Further optimizing the trap parameters from this point until the individual ions are observable proved difficult. It was observed that the cooling efficiency is closely related to the size of the ion cloud being trapped. Some large ion clouds do not condense for prolonged periods of time, and will remain dim regardless of the frequencies or intensities of the laser. There are several possible explanations as to why the Doppler cooling method fails to condense the ion cloud. One possible explanation for this is that the trap electrodes are picking up electrical noise from its surroundings. Electrical noise may distort potential within the trap, thus possibly affecting the trap stability and heating up the ions.

Another explanation for the inefficiency of the cooling system is the micromotion of the ions. In Section 2.2 the micromotion is described as the tiny oscillatory motion caused by the fast fluctuation of the RF potential. The micromotion of the ions may adversely affect the cooling systems under certain situations. Ideally, trapped ions would be confined in the immediate area surrounding the trap center, which is the nodal point of the RF potential and where the amplitude of the fluctuation of the RF is minimized. However, if a stray field were to displace the ions sufficiently far away from the nodal point of the RF potential, then the amplitude of the fluctuations acting on the ions would be large and the micromotion will be large. From the point of view of the ion, such excess micromotion can cause the creation of sidebands to the 493nm laser, which may heat the ions up if they are in the blue detuned region. This heating effect may be reduced by compensating for the stray field, or reducing the frequency of the RF[4]. A reduction in the frequency of the RF however, will entail a redesign and reconstruction of the RF driver. Compensating for the stray field can be achieved by shifting the ion around usby applying additional DC biases onto each individual electrode, end cap or base plate. This is tweaked until the trapped ions are stable.

There are several possible sources for stray fields within the trap which may cause this increase in the micromotion. Stray fields can be the result of asymmetries in the design of the trap - for example, the bottom electrodes are closer to the base plate, and the electrodes on one side are closer to the oven and electron gun housing - which can distort the potential field and displace the ions. Another possibility is that charge is being stored at the base of the Paul trap, which is made of the dielectric, macor. Over time, the macor base may store electrons from the electron gun or from the photoelectric emissions from the trap surface, eventually building up enough charge to introduce a significant stray field.

When the ions are stabilized, the operating current of the barium oven is gradually turned down from 5A to about 3.6A. At this point, the number of trapped ions are reduced and small ion chains are eventually observed with individual ions being clearly resolved. The initial lifetime of the trapped ions is initially only 15mins, but further optimization of the trap eventually lead to trap lifetimes of the order of several days. A picture of a small ion chain is shown in Figure 19. The ions line up in a chain because the confinement in the axial direction of the trap (along the end caps) is weaker as compared to the confinement along the radial directions. The gap in the middle of the ion chain shown in Figure 19 is due to the presence of a dark isotope of barium which does not participate in the fluorescence.

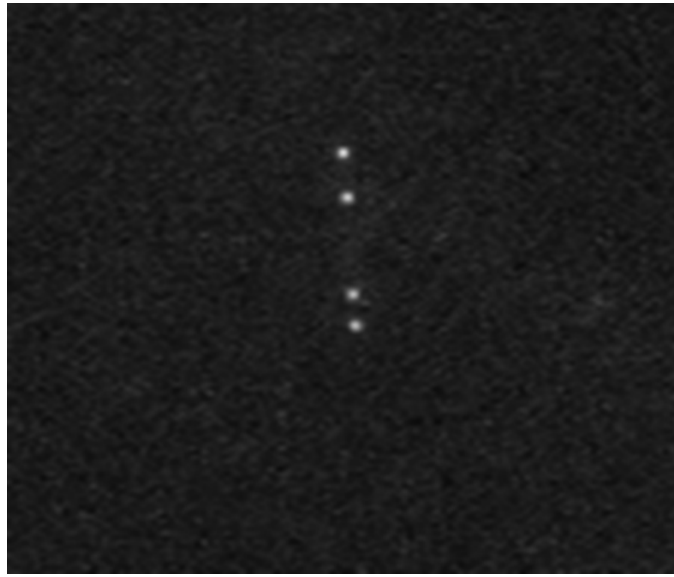


Figure 19: A picture of the small ion chain taken near the end of this project

Chapter 5

5 Conclusion, Summary of Experience and Future Directions of The Project

This ion trapping exercise concludes with the successful confinement of small chains of barium ions using a linear Paul trap. At this juncture, although ions can now already be reliably loaded into the trap, the stability and the lifetimes of the trap are continually being refined, and improvements to the trap in areas such as the ion stability and trap life times are still being made.

There were many difficulties encountered during the initial attempts to load ions into the trap, most of them being technical in nature. The most obvious difficulty in the entire process is to identify the reasons why the Paul trap is not working when should. The main reason for this is that the trap itself is housed within a vacuum system, and it is not possible to probe inside the chamber in order to see what the problem is. Several indirect methods were devised to this end, such as the collection of electrons using the trap electrodes, to test the electrical connections within the trap. Another notable difficulty we had while trapping ions were with the barium oven being blocked by oxide layers. Several different designs of the barium oven were tested before a reliable design eventually emerged. Once all the technical difficulties were resolved, the trapping of ions then proceeded relatively smoothly.

The immediate next step of the project is to isolate the various isotopes of barium being trapped. For the purpose of this ion trapping exercise, we were not selective over the kinds of barium ions that were within the trapping region.

While our detection system only covers the most common isotope of barium, Barium 138, the existence of other isotopes can readily be inferred from gaps in otherwise regular chains of ions. Barium 138 has nuclear spin zero, so it does not have the necessary hyperfine splitting which is required for state sensitive detection. The goal is to eventually be able to trap Barium 137, which has nuclear spin $1/2$. Once Barium 137 is trapped, this trap will serve as a test bed for ground state cooling and state selective detection techniques needed for future work. Additionally this work will provide a convenient ionic frequency reference within the laboratory. One frustrating problem in initial attempts to trap ions was insufficient knowledge of the absolute laser frequency due to the lack of a suitable atomic reference. Now that ions have been observed, unknown offsets in the transfer cavity locks can be calibrated.

Another objective of this project was to construct an ion trap that could incorporate an optical cavity for cavity QED experiments. The trap used here provides plenty of optical access for a cavity and the associated cooling lasers. Although the trap used here has dimensions that are larger than desired for the inclusion of a cavity, it is readily reduced in size. Towards this end, a second linear Paul trap has been constructed which incorporates all of the features of the trap developed in this project, with the exception of its smaller dimensions. This trap is pictured in Figure 20, and is essentially the same design used here, except that the cooling lasers enter the trap vertically. Two piezoelectric transducers are placed along the horizontal axis perpendicular to the axial direction of the trap on which cavity mirrors will be mounted. The piezos are each able to shear along the axis for several hundred nanometers, allowing for the fine tuning of the cavity resonance and the position of the ion along the cavity axis. The cavity base is mounted on an attocube so that the cavity can be displaced vertically relative to the ion to ensure the ion overlaps with the cavity mode.

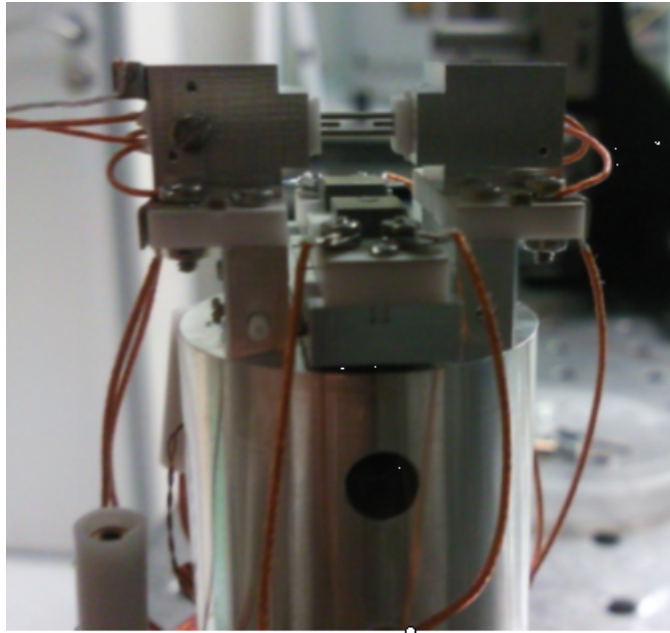


Figure 20: The microtrap constructed for the next phase of the ion trapping experiments.

This trap is currently being tested within a high vacuum environment. The work done in this project has eliminated many of the technical issues encountered when trapping ions for the first time and is likely to considerably speed up the setup of this new trap.

References

- [1] *Proceedings of the 35th Annual Symposium on the Foundations of Computer Science*, New York, 1994. Computer Society Press.
- [2] P.F. Griffin A.V. Steele, L.R. Churchill and M.S. Chapman. Photoionization and photoelectric loading of barium ion traps. *Physical Review A*, 75, 2007.
- [3] D.J. Berkeland and M.G. Boshier. Destabilization of dark states and optical spectroscopy in zeeman-degenerate atomic systems. *Physical Review A*, 65:1–12, 2002.
- [4] J. C. Bergquist W. M. Itano D. J. Berkeland, J. D. Miller and D. J. Wineland. Minimization of ion micromotion in a paul trap. *JOURNAL OF APPLIED PHYSICS*, 83(10), 1998.
- [5] S. Earnshaw. On the nature of the molecular forces which regulate the constitution of the luminiferous ether. *Trans. Camb. Phil. Soc.*, 7:97–112, 1842.
- [6] Randall G. Hulet F.B. Dunning, editor. *Atomic, Molecular, and Optical Physics: Charged Particles*, volume 29A. Academic Press, Inc., 1995.
- [7] Christopher J. Foot. *Atomic Physics*. Oxford University Press, 2005.
- [8] Wayne M. Itano and D.J. Wineland. Laser cooling of ions stored in harmonic and penning traps. *Physical Review A*, 25:35–54, 1982.
- [9] F. Buchinger A.C. Mueller R. Neugart K. Went, S.A. Ahmad and E.W. Otten. Relativistic j-dependence of the isotope shift in the 6s-6p doublet of ba ii. *Z. Phys. A - Atoms and Nuclei*, 318:125–129, 1984.

- [10] H. Karlsson and U. Litzen. Revised ba i and ba ii wavelengths and energy levels derived by fourier transform spectroscopy. *Physica Scripta*, 60:321–328, 1999.
- [11] K. Abdullah L. Haarsma and G. Gabrielse. Extremely cold positrons for antihydrogen production. *Hyperfine Interactions*, 76:143, 1993.
- [12] S.N. Chatterjee L. K. Jha and B.N. Roy. Electron impact double ionization of ba and ba+. *Pramana Journal of Physics*, 43:169–174, 1994.
- [13] H. Volten M.D. Davidson, L.C. Snek and A. Donszelmann. Oscillator strengths and branching ratios of transitions between low-lying levels in the barium ii system. *Astronomy and Astrophysics*, 255:457–458, 1992.
- [14] E. Fischer W. Paul, O. Osberghaus. Forschungsberichte des wirtschaft und verkehrministeriums nordrhein westfalen. *Westdeutscher Verlag, Koln*, 415, 1958.
- [15] Anatol I. Zverev. *Handook of Filter Synthesis*. Wiley, 1967.

Appendix A

The Q Factor

The Q factor of a general system under forced oscillation is generally defined as such:

$$Q = 2\pi \frac{\text{Energy Stored at Resonance}}{\text{Energy Dissipated per cycle at Resonance}} \quad (21)$$

In order to find out the Q factor of the resonator, we first consider a general damped harmonic oscillator under the influence of a periodic force, such as a pendulum oscillating in air acting under a periodic force, or in our case, an L-C circuit. The general form of the differential equation is given by

$$\frac{d^2x}{dt^2} + b\frac{dx}{dt} + kx = F \cos(\Omega t) \quad (22)$$

where x is the displacement of the oscillation, b is the damping coefficient of the oscillator, k is the force constant of the oscillation, F is amplitude of the external driver, and Ω is the frequency of the driver. The general solution for this forced oscillation is then

$$x = Ae^{-\frac{b}{2}t} \cos(\omega t + \phi) + \frac{b\Omega}{(k - \Omega^2)^2 + (b\Omega)^2} \sin(\Omega t) + \frac{k - \Omega^2}{(k - \Omega^2)^2 + (b\Omega)^2} \cos(\Omega t) \quad (23)$$

$$\omega = \sqrt{k - \frac{b^2}{4}} \quad (24)$$

As $t \rightarrow \infty$ and the oscillating system approaches a steady state, the first term of Equation 23 will eventually become negligible. The resulting amplitude of

the driven oscillation using the remaining terms will then be

$$A = \frac{F}{\sqrt{(k - \Omega^2)^2 + (b\Omega)^2}} \quad (25)$$

From which it is simple to find the stored energy of the oscillator, which is given by the following:

$$\begin{aligned} \text{Energy Stored} &= \frac{1}{2}kA^2 \\ &= \frac{1}{2}k \frac{F^2}{(k - \Omega^2)^2 + (b\Omega)^2} \end{aligned} \quad (26)$$

In order to find an expression for the Q, we would need to find out the amount of energy dissipated per cycle (see Equation 21), in addition to the amount of energy stored. At the steady state, the amount of energy dissipated per cycle must be equivalent to the amount of work done by the external driver per cycle. From this we can obtain the following expression for the energy dissipated:

$$\begin{aligned} \text{Energy Dissipated Per Cycle} &= \int_{1 \text{ cycle}} F \cos(\Omega t) dx \\ &= \frac{2\pi F^2 \Omega}{2\sqrt{(k - \Omega^2)^2 + (b\Omega)^2}} \end{aligned} \quad (27)$$

As we are primarily concerned with the system at resonance, assuming $\Omega = \omega$, Equation 26 and Equation 27 would lead to the following expression for Q:

$$Q = \frac{1}{b} \quad (28)$$

At this point Equation 28 explains why Q is a measure of how under-damped an oscillating system is. As Q is inversely proportional to the damping coefficient, small damping coefficients lead to a larger Q and vice versa. By extension, it

can also be inferred from here that the amplitude of the forced oscillation is larger for higher values of Q . For example, in the simplest case of an oscillating pendulum, the pendulum would oscillate at a much larger amplitude under a forced oscillation surrounded by air as compared to when it is under a forced oscillation when surrounded by oil. This the damping coefficient in oil is much larger. In much a similar manner, a higher Q value therefore leads to a larger voltage amplification for the case of the resonator in an L-C circuit. Further, we can infer the relationship between the oscillating amplitude and the Q factor from Equation 25. By assuming that the external driver is operating at resonance, $\Omega = \omega$, and that the natural frequency of oscillation is approximately equal to the damped oscillation, $k \approx \omega^2$ (which is true in a lightly damped system), then the amplitude of the oscillation is simply given by:

$$\begin{aligned} A &= \frac{F}{\omega} Q \\ &\propto Q \end{aligned}$$

Which suggests a linear relationship between the Q factor and the amplitude of the oscillation in lightly damped systems.

However, it is often difficult to directly measure the damping coefficient of the system, which is the case for our resonator system. In order to resolve this, we now make an observation that Equation 26, which is the energy distribution of the system in terms of Ω , is approximately a Lorentzian distribution at points of Ω close to the resonance frequency ω . This Lorentzian distribution in the Energy-Frequency domain has a line width $\Gamma = b\omega$, which implies an alternative expression for the Q factor:

$$Q = \frac{\omega}{\Gamma} \tag{29}$$

However, Γ is the full-width half maximum (FWHM) within the Energy-Frequency domain of the oscillating system, which presents its own difficulties. It is more convenient in a practical sense to re-express the expression in terms of the Amplitude-Frequency domain as in a laboratory environment, amplitude measurement devices such as oscilloscopes are commonly used. Another equivalent expression for Q is then

$$Q = \frac{\omega}{\Delta_{3dB}} \quad (30)$$

where Δ_{3dB} is the width of the Amplitude-Frequency distribution at the 3dB point, and ω is simply the resonant frequency of the system. Therefore, by measuring the deviation from the resonant frequency at the 3dB point of the amplitude, the Q for the system can easily be measured. For the resonator used in this experiment, this can be readily achieved by using a digital oscilloscope to measure the amplitude and the frequency of the EMF induced in a wire placed near the end of the helical inner conductor.